

Cite this: *Dalton Trans.*, 2021, **50**, 1604Received 29th October 2020,  
Accepted 14th January 2021

DOI: 10.1039/d0dt03726e

rsc.li/dalton

## Designed sol–gel precursors for atomically dispersed Nb and Pb within TiO<sub>2</sub> as catalysts for dihydroxyacetone transformation†

Antonio de Brito Santiago Neto,<sup>a,b</sup> Márcia Gabriely Alves da Cruz,<sup>a,b</sup> Erwann Jeanneau,<sup>c</sup> Alcineia Conceição Oliveira,<sup>b</sup> Nadine Essayem<sup>a</sup> and Shashank Mishra<sup>†</sup> 

The 'bottom-up' synthesis of homogeneously doped metal oxide nanoparticles (NPs) with precision at the atomic/molecular level offers many advantages. We report here the synthesis, structural characterization and hydrolytic behavior of new *N*-methyl-diethanolamine-modified precursors of Ti(IV), Nb(V) and Pb(II) and their application as excellent sol–gel precursors for obtaining atomically dispersed Nb and Pb within TiO<sub>2</sub> having high surface areas (253–355 m<sup>2</sup> g<sup>-1</sup>) and tunable acidic properties. Preliminary results on the use of these doped TiO<sub>2</sub> as water-tolerant catalysts in transforming dihydroxyacetone to lactic acid are presented.

Dihydroxyacetone (DHA) is an attractive triose sugar currently obtained by the valorization of crude glycerol from the production of biodiesel.<sup>1–3</sup> DHA is used as an active ingredient in sunless tanning lotions and as a precursor for the preparation of an increasingly sought-after commodity chemical, lactic acid (LA).<sup>4,5</sup> The DHA transformation into LA proceeds *via* dehydration of the DHA triose yielding pyruvaldehyde (PA) as an intermediate – a first step described to be catalyzed by both Lewis and Brønsted acids (Scheme 1). The subsequent rehydration step of pyruvaldehyde to lactic acid is reported to be promoted by Lewis acids where key hydride transfer shifts are required.<sup>3,5,6</sup> The use of heterogeneous Brønsted and Lewis

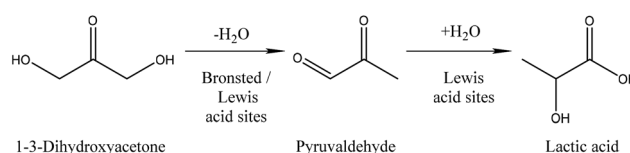
acid catalysts has been reported in the literature, with some applications to lactate synthesis in alcoholic medium.<sup>7–9</sup> Recent studies have reported the strong dependence of the acidic nature of the catalysts when the reaction is carried out in water for lactic acid production.<sup>3,8,10</sup> The 'bottom-up' synthesis of nanomaterials using well-defined molecular precursors has many advantages over traditional synthetic routes including access to these materials at much lower temperatures.<sup>11</sup> The advantages of the sol–gel (SG) process as a soft solution route for the elaboration of homogeneously doped metal oxide nanomaterials are well documented.<sup>12</sup> Metal alkoxides are the preferred sol–gel precursors for metal oxide ceramics<sup>13</sup> and catalytic materials,<sup>14</sup> but the use of classical metal alkoxides in the SG process is unattractive due to their extremely high susceptibility towards hydrolysis and poor stability of the resulting colloidal solutions. The modification of classical metal alkoxides by functional alcohols bearing additional ether or amino functionalities not only alter their physical and chemical properties such as hydrolysis susceptibility, solubility, viscosity, *etc.* but also, due to their action as surfactants, stabilize the colloidal solutions obtained during hydrolysis.<sup>15</sup> In this regard, we have shown previously that aminoalcohols are not only easily modified to modulate their steric and electronic properties,<sup>16</sup> but their metal derivatives are very attractive sol–gel precursors for metal oxide nanomaterials because of the favorable hydrolysis and condensation characteristics and their transformation into oxides at relatively low temperatures.<sup>17–20</sup> These characteristics and the interesting structural features that play a role in determining the pro-

<sup>a</sup> Université Claude Bernard Lyon 1, CNRS, UMR 5256, Institut de Recherches sur la Catalyse et l'Environnement de Lyon (IRCELYON), 2 avenue Albert Einstein, 69626 Villeurbanne, France. E-mail: shashank.mishra@irceylon.univ-lyon1.fr; Fax: +33-472445399; Tel: +33 472445322

<sup>b</sup> Universidade Federal do Ceará, Campus do Pici-Bloco 940, Departamento de Química Analítica e Fisioquímica, 60.000.000 Fortaleza, Ceará, Brazil

<sup>c</sup> Université Claude Bernard Lyon 1, Centre de Diffraction Henri Longchambon, 5 rue de La Doua, 69100 Villeurbanne, France

† Electronic supplementary information (ESI) available: Experimental section, FT-IR and single crystal X-ray refinement data of the new precursors, TG-DTG curves of as-prepared undoped and Nb- or Pb-doped TiO<sub>2</sub> NPs obtained from the hydrolysis of the precursors, Raman spectra, STEM images and N<sub>2</sub> adsorption-desorption isotherms of the Nb- and Pb-doped TiO<sub>2</sub>, DHA conversion profiles catalyzed by these undoped or doped TiO<sub>2</sub> and 3 X-ray crystallographic files in CIF format. CCDC 1558717, 2034796 and 2013426 for **1**, **2a** and **3**, respectively. For ESI and crystallographic data in CIF or other electronic format see DOI: 10.1039/d0dt03726e



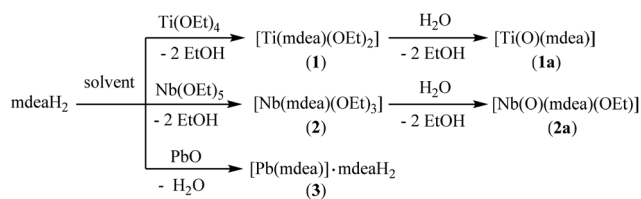
**Scheme 1** Dihydroxyacetone conversion to lactic acid *via* pyruvaldehyde formation.

properties of the final material produced have prompted us to investigate the designed metal aminoalkoxides for the solution- and vapor-phase synthesis of metal oxides.<sup>15–20</sup> By extending the above studies, we report here the synthesis, structural characterization and hydrolytic behavior of new *N*-methyldiethanolamine-modified precursors of titanium(IV), niobium(V) and lead(II). The choice of these metals was motivated by the aim to synthesize water-tolerant TiO<sub>2</sub> nanoparticles doped with Nb or Pb, dispersed homogeneously and at the atomic scale within the TiO<sub>2</sub> matrix to tune its catalytic acid–base properties. Indeed, the water tolerance of TiO<sub>2</sub> is well documented in the field of heterogeneous catalysis, where it has been employed as a stable support of noble metals or as solid Lewis acids for carbohydrate conversion.<sup>21</sup> The access to the designed metal aminoalkoxide precursors appears as a unique tool to boost the Lewis acidity of nanometric TiO<sub>2</sub> in a controlled way, *via* its doping with low amounts of metal centers capable of providing Lewis acid centers. The oxides of Nb and Pb were chosen due to their reported Lewis acidity.<sup>22</sup> The use of these derivatives as sol–gel precursors not only resulted in an excellent homogeneous dispersion of the dopant Nb or Pb within TiO<sub>2</sub> at the atomic level but also ensured a high surface area in the range of 250–355 m<sup>2</sup> g<sup>−1</sup> and an enhanced Lewis acidity as demonstrated by their application as excellent water-tolerant acid catalysts for the model reaction of dihydroxyacetone conversion into lactic acid.

New titanium(IV) and niobium(V) aminoalkoxides **1** and **2** were synthesized by ethoxo-aminoalkoxo exchange reactions in toluene using [Ti(OEt)<sub>4</sub>]/[Nb(OEt)<sub>5</sub>] and *N*-methyldiethanolamine as starting reagents, whereas lead(II) derivative **3** was prepared by refluxing PbO with *N*-methyldiethanolamine in toluene (Scheme 2). While the derivatives **1** and **3** are crystalline solids, the niobium(V) derivative **2** is a viscous oil. The heteroleptic derivatives **1** and **2**, which have residual ethoxide groups, were also studied for their microhydrolysis behavior, which produced oxo clusters of the compositions [Ti(O)(mdea)] (**1a**) and [Nb(O)(mdea)(OEt)] (**2a**), respectively (Scheme 2). While the heteroleptic derivatives **1** and **2** show good solubility in common organic solvents such as toluene, THF, chloroform and alcohols, the homoleptic derivative **3** and the oxo-clusters **1a** and **2a** are insoluble in hexane, only moderately soluble in chloroform but soluble in alcohols.

Crystals suitable for single crystal X-ray studies of **1**, **1a**, **2a** and **3** were obtained as described in the Experimental section in the ESI.† In the dimeric structure of [Ti<sub>2</sub>(μ-mdea)(mdea)

(μ-OEt)(OEt)<sub>3</sub>] **1**, which crystallizes with a solvated ethanol molecule in the space group *P*1̄, two titanium centers are bridged by one alkoxide arm of a bridging–chelating mdea ligand and one ethoxide group (Fig. 1a). The remaining alkoxide arm and the nitrogen center of the bridging–chelating mdea ligand are coordinated to the Ti2 atom, which is additionally substituted by two terminal OEt ligands. The other titanium atom (Ti1) in the dimer is coordinated to one chelating mdea ligand and a terminal OEt group. Thus, each titanium is six-coordinated with a TiO<sub>5</sub>N coordination sphere. The terminal ethoxy groups are most strongly bound [Ti–O<sub>terminal</sub> 1.812(2)–1.818(2) Å], followed by the aminoalkoxide [Ti–O<sub>mdea</sub> 1.860(2)–1.899(2) Å], while the bridging interactions are, unsurprisingly, weaker [Ti–O<sub>bridging</sub> 2.018(2)–2.057(2) Å]. The Ti–N bond distances, 2.349(3)–2.374(3) Å, are typical of these species. The octahedral environment around Ti1 and Ti2 centers is considerably distorted as indicated by the *cis* O–M–O and O–M–N angles ranging from 69.8(8) to 109.2(1)°. These discrete dimeric entities do not have any considerable interaction among themselves but form H-bonding (2.977 Å) with the solvated EtOH molecules. Titanium(IV) derivatives with the *N*-methyldiethanolamine ligand have previously been studied.<sup>23–25</sup> While the reaction of Ti(OPr<sup>*i*</sup>)<sub>4</sub> with 2 equivalents of mdeaH<sub>2</sub> ligand under reflux afforded a fully substituted product [Ti(mdea)<sub>2</sub>],<sup>23</sup> its reaction with 1 equivalent of mdeaH<sub>2</sub> actually gave an unsymmetrical dimer [Ti<sub>2</sub>(mdea)(OPr<sup>*i*</sup>)<sub>6</sub>] (Scheme S1†).<sup>24</sup> This reaction was thought to proceed through a transitory coordinatively unsaturated and insufficiently shielded species [Ti(mdea)(OPr<sup>*i*</sup>)<sub>2</sub>] (**A**), which further reacted with Ti(OPr<sup>*i*</sup>)<sub>4</sub> to finally afford a sterically controlled product [Ti<sub>2</sub>(mdea)(OPr<sup>*i*</sup>)<sub>6</sub>]. The OPr<sup>*i*</sup> groups, which are sterically more crowded than the OEt groups, apparently prevented the more straightforward dimerization of **A**, which would also have given a coordinatively saturated product. On replacing OPr<sup>*i*</sup> with less-hindered OEt, dimerization becomes feasible as confirmed by the isolation and structural characterization of **1** here. This structure, therefore, completes a missing link in the library of titanium derivatives with the *N*-methyldiethanolamine ligand, which is an important modifier in the sol–gel procedure.<sup>15</sup> The structure of **1** also underlines the versatility in the bonding capabilities of the mdea ligand, which adopts here both chelating and bridging modes. The unit cell parameters of **1a** matched well with the previously reported [Ti<sub>6</sub>(O)<sub>6</sub>(mdea)<sub>6</sub>] obtained through the hydrolysis of the homoleptic derivative [Ti(mdea)<sub>2</sub>].<sup>25</sup> Therefore, no further data were collected for this compound. The molecular structure of [Nb<sub>4</sub>(μ-O)<sub>4</sub>(mdea)<sub>4</sub>(OEt)<sub>4</sub>] (**2a**) is based on a cyclic Nb<sub>4</sub>O<sub>4</sub> core (Fig. 1b). It crystallizes in the monoclinic space group *I*2. Four niobium atoms and four bridging oxo ligands lie in a plane forming a square with two *trans* Nb...Nb distances being almost equal (5.383 and 5.386 Å). The niobium-oxo bond lengths vary from 1.831(7) to 2.015(7) Å, thus resulting in a slightly asymmetrical Nb<sub>4</sub>O<sub>4</sub> ring. The bridging oxo ligands are slightly shifted out from the square sides, as indicated by an angle of about 165° at them. Each niobium centre has a chelating mdea ligand, bonded *via* two oxygen atoms and a nitrogen atom, and a terminal ethoxo ligand to



**Scheme 2** Synthesis and partial hydrolysis behavior of new *N*-methyl diethanolamines of Ti(IV), Nb(V) and Pb(II).

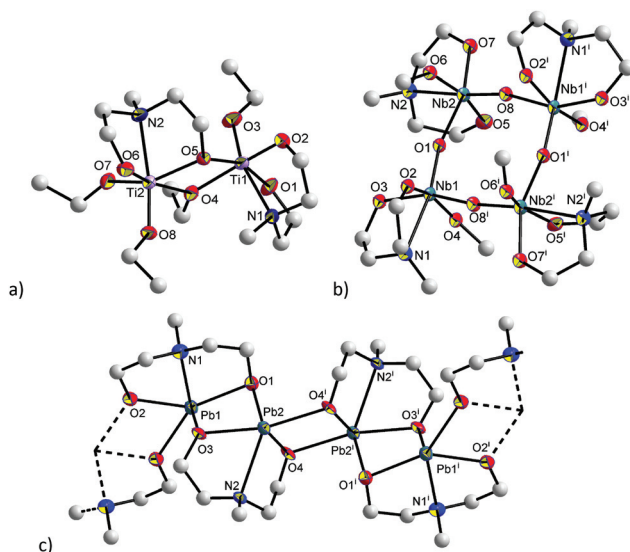


**Fig. 1** Perspective views of **1** (a), **2a** (b) and **3** (c) with displacement ellipsoids drawn at the 30% probability level. Carbon atoms are drawn as ball and stick and the H-atoms on alkyl groups are omitted for clarity. Selected bond lengths (Å) and angles (°): (**1**) Ti1–O1 1.899(2), Ti1–O3 1.818(2), Ti1–O4 2.057(2), Ti1–O5 2.053(2), Ti1–N1 2.374(3), O4–Ti1–O5 69.78(8), N1–Ti1–O3 164.42(10), O1–Ti1–O2 104.55(11); (**2a**) Nb1–O8<sup>i</sup> 2.015(7), Nb2–O8 1.831(7), Nb2–O6 1.771(11), Nb2–O5 2.027(12), Nb1–N1 2.442(11), Nb–N2 2.459(10), O1–Nb1–N1 168.0(5), O2–Nb1–O4 160.1(4), O2–Nb1–O8<sup>i</sup> 76.0(5), Nb1–O1–Nb2 164.9(4), Nb2–O8–Nb1<sup>i</sup> 165.1(6); (**3**) Pb1–O1 2.676(7), Pb2–O4 2.174(6), Pb1–N1 2.569(9), Pb2–N2 2.763(8), O2–Pb1–O1 134.6(2), O2–Pb1–N1 69.5(3), Pb2–O1–Pb1 102.4(2), Pb2–O4–Pb2<sup>i</sup> 110.1(3). Symmetry elements: (**2a**) (i)  $1 - x, y, 1 - z$ ; (**3**) (i)  $1 - x, 1 - y, 1 - z$ .

complete the 6-coordination sphere around it. The Nb–O bond lengths of these ligands vary from 1.771(11) to 2.027(12) Å, while the Nb–N bond lengths are in the range of 2.442(11)–2.459(10) Å. While the Nb–O distances are in agreement with the literature,<sup>26</sup> the Nb–N distances are slightly longer in **2a** than those found in related 6-coordinated Nb(v) complexes with N-containing ligands.<sup>27</sup> The structure of the solvated compound [Pb(mdea)]·mdeaH<sub>2</sub> (**3**) reported here is quite similar at the molecular level to the previously described non-solvated [Pb(mdea)],<sup>28</sup> although both crystallize in different space groups (*I2/a* and *C2/c*, respectively) and, therefore, have different molecular packings. Similar to the non-solvated [Pb(mdea)], the structure of the compound **3** also corresponds to a polymer based on 5-coordinate lead centers having a trigonally distorted octahedral stereochemistry (if the electron lone pairs are taken into account) (Fig. 1c). The Pb–O [2.174(6)–2.676(7) Å], Pb–N [2.569(9)–2.763(8) Å] and Pb...Pb [3.86–3.91 Å] distances also compare well with the reported structure.<sup>28</sup> While the IR spectra of the new mixed-ligand derivatives **1** and **2** exhibit characteristic bands of the parent ligands, *N*-methyldiethanolamine and ethoxide, the homoleptic **3** and oxo-derivative **2a** show only the bands for the parent aminoalkoxide ligand (Fig. S1†). All the bands of the mdea ligand appears as twice in close vicinity for **3**, which is consistent with its crystal structure having a free mdeaH<sub>2</sub> ligand in its lattice. The solvated nature of this species

as well as of **1** is further confirmed by the presence of absorption bands due to  $\nu(\text{OH})$  in the 3100–3500 cm<sup>-1</sup> region. All the new derivatives reported here also show new bands in the 675–415 cm<sup>-1</sup> region for  $\nu(\text{M–O})$  and  $\nu(\text{M–N})$  stretching vibrations. The room temperature <sup>1</sup>H NMR spectra of these new derivatives are either simple or poorly resolved, indicating a fluxional behavior for them under these conditions. The signals due to OEt and/or mdea ligands appear in the regions and integrated intensity ratios expected for them, although their multiplicity is sometimes not so well resolved [e.g.,  $\delta$  1.23 (CH<sub>3</sub>CH<sub>2</sub>O), 2.29 (N–Me), 2.61 (NCH<sub>2</sub>), 3.67 (OCH<sub>2</sub>) and 4.32 ppm (CH<sub>3</sub>CH<sub>2</sub>O) in **1**]. This fluxional process does not cease even at low temperature.

The precursor **1** was hydrolyzed using a modified procedure of a previously published report on obtaining metal oxides with high surface areas.<sup>29</sup> In a typical procedure, a toluene solution of **1** was added to a calculated amount of an aqueous solution of acetic acid, followed by refluxing and aging for 3 h. The powder obtained after the removal of the solvents using a rotary evaporator was capped by *N*-methyldiethanolamine ligand, as confirmed by the FT-IR and TG-DTA studies on it (Fig. S2†). Since the as-obtained NPs were poorly crystallized, these were calcined at 500 °C to remove the remaining of the organics and to make them well crystallized. The XRD of this calcined sample revealed it to be well crystallized with all the peaks indexing well with the PDF file 00-021-1272 of the pure anatase phase (Fig. 2). To obtain Nb- or Pb-dispersed TiO<sub>2</sub>, the precursors **1** and **2** (or **1** and **3**) were taken in an appropriate molar ratio in toluene, stirred for 1 h to obtain a homogeneous solution, and then hydrolyzed as described above. The as-obtained NPs, which are capped with the *N*-methyldiethanolamine ligand (Fig. S3 and S4†), were calcined at 500 °C for 4 h for the complete removal of the organic ligands. The XRD peak positions of the doped Nb/TiO<sub>2</sub> or Pb/TiO<sub>2</sub> were the same as that of the undoped TiO<sub>2</sub>, with all the peaks indexing well with the pure anatase phase (Fig. 2). However, these peaks were slightly broader and less intense,

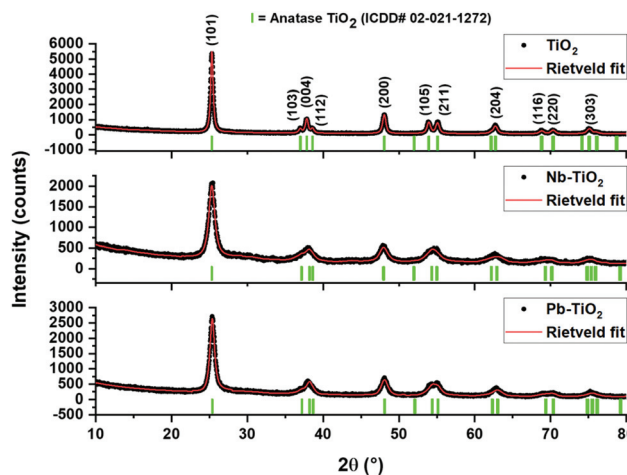


**Fig. 2** Powder XRD patterns of undoped TiO<sub>2</sub>, Nb/TiO<sub>2</sub> and Pb/TiO<sub>2</sub> NPs obtained from the hydrolysis of **1** alone or a mixture of **1** + 10% **2** or **1** + 10% **3**, respectively, followed by calcination at 500 °C.

indicating a lower degree of crystallization in Nb/TiO<sub>2</sub> and Pb/TiO<sub>2</sub>. No peaks for doped niobium or lead oxides could be observed in the XRD patterns, thus suggesting the ultradisersion of these species on the surface and/or within the TiO<sub>2</sub> matrix. The Rietveld refinement of powder XRD of these samples reveals that the TiO<sub>2</sub> lattice becomes more strained upon doping with Nb or Pb, even though there is no significant change in the lattice parameters (Table S2†). The Raman spectra, which display typical vibrational modes of the anatase TiO<sub>2</sub> at 144 cm<sup>-1</sup> (E<sub>g</sub>), 195 cm<sup>-1</sup> (E<sub>g</sub>), 394 cm<sup>-1</sup> (B<sub>1g</sub>), 514 cm<sup>-1</sup> (A<sub>1g</sub> + B<sub>1g</sub>), and 634 cm<sup>-1</sup> (E<sub>g</sub>), also show a slight broadening and decreased intensity for the Nb/TiO<sub>2</sub> and Pb/TiO<sub>2</sub> catalysts, thus indicating a decrease in the crystallinity as well as an increase in the defects for these samples (Fig. S5†). Moreover, the absence of any detectable vibrations due to niobium or lead oxide confirms the extremely high dispersion of Pb and Nb within the TiO<sub>2</sub> matrix. These studies also suggest that the niobium and lead atoms are in the Nb<sup>5+</sup> and Pb<sup>2+</sup> states, respectively. The atomic-level ultradisersion in these catalysts is further confirmed by the high-resolution STEM images, which show the absence of particles larger than 2 nm on the two doped TiO<sub>2</sub> samples (Fig. 3, S6†). While the Pb dopant is ultradispersed in TiO<sub>2</sub> at the atomic level, the dispersion of the Nb dopant within the TiO<sub>2</sub> matrix is slightly less homogeneous, as marked by the coexistence of isolated atoms and clusters of varying sizes (0.5 nm to 2 nm). The above studies indicate a major inclusion of Nb and Pb inside the TiO<sub>2</sub> lattice although a part of these species, especially for Nb, also exists as small clusters of less than 2 nm, well dispersed on the TiO<sub>2</sub> nanoparticles, thanks largely to the milder sol-gel conditions employed here for the synthesis of these catalysts.<sup>30</sup> The N<sub>2</sub> adsorption-desorption isotherms of the two doped samples Nb/TiO<sub>2</sub> and Pb/TiO<sub>2</sub> are typical of mesoporous materials, displaying type IV isotherms with hysteresis in the range of 0.4 < P/P<sub>0</sub> < 0.8 (Fig. S7†). A significantly high BET surface area for the two doped samples (253 and 355 m<sup>2</sup> g<sup>-1</sup> for Nb/TiO<sub>2</sub> and Pb/TiO<sub>2</sub>, respectively, as against 40 m<sup>2</sup> g<sup>-1</sup> for the undoped TiO<sub>2</sub>) can be attributed to the smaller crystallite size (9.9 and 16.6 nm in Nb-TiO<sub>2</sub> and in Pb-TiO<sub>2</sub>, respectively, *versus* 20 nm in undoped TiO<sub>2</sub>) and the empty space among the loosely coagulated primary particles. The properties of the final materials depend on the nature of the precursors and the preparative methods employed. The high surface area and atomic dispersion observed here are due to the surface passivating effects of the *N*-methyldiethanol amine ligand and the sol-gel process employed resulting in small nanoparticles and the imperfect packing of these nanoparticles. Achieving finely dispersed doped metal oxide nanoparticles with a remarkably high surface area here thus validates the use of the designed precursors and the modified sol-gel procedure.

The above-obtained highly dispersed Nb/TiO<sub>2</sub> and Pb/TiO<sub>2</sub> catalysts having high surface areas were evaluated for the model reaction of dihydroxyacetone transformation into lactic acid and compared to the undoped TiO<sub>2</sub> catalyst. The evolutions of DHA consumption as a function of reaction time for different solids are shown in Fig. 4a. It is noteworthy that, due

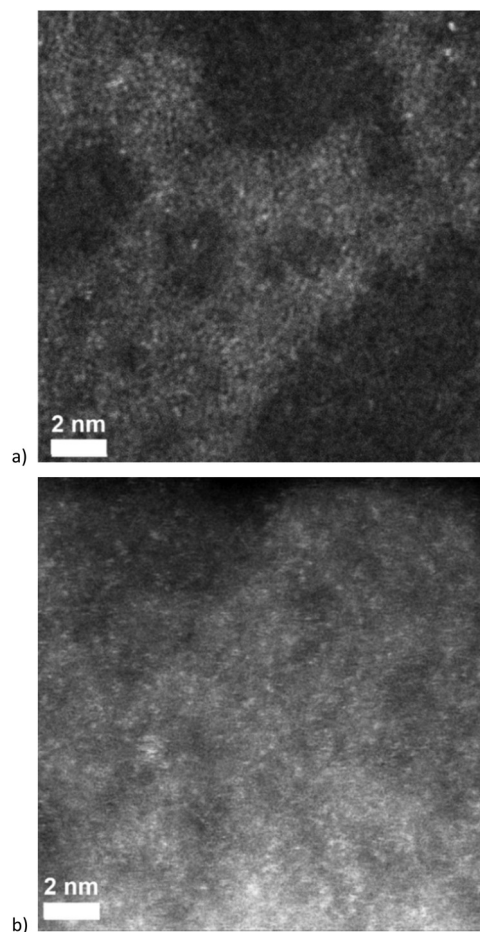


Fig. 3 STEM-ADF images of Nb/TiO<sub>2</sub> (a) and Pb/TiO<sub>2</sub> (b).

to the homogeneous dispersion of the acidic metal centers in the TiO<sub>2</sub> framework, the DHA consumption increases significantly up to 89% conversion for the Nb/TiO<sub>2</sub> catalyst after 4 hours of reaction. Over Pb/TiO<sub>2</sub>, a lower DHA conversion is achieved, which is 75% after 4 h. These values are well above the 49% conversion after 4 h, obtained for dopant-free TiO<sub>2</sub>. The initial rates of DHA conversion (Table 1) increased by factors of 1.6 and 2.7 upon doping with Pb and Nb, respectively, without correlation with the surface enhancement. This enhanced activity can be explained by the superficial acidic properties achieved through the doping of TiO<sub>2</sub> with niobium and lead. According to the generally accepted mechanism (*cf.* Scheme 1), pyruvaldehyde (PA) is the intermediate product that is produced by DHA dehydration catalyzed by the Brønsted or Lewis acid sites, whereas the final product lactic acid (LA) is formed by hydration of PA and further hydride transfers promoted by the Lewis acid sites solely (Fig. S8†).<sup>5,8,31</sup> The production of lactic acid is due to the presence of accessible Lewis acid sites in the solid structure, and the increased LA yield with the progress of the reaction is related to the increase of Lewis acidity of TiO<sub>2</sub> after doping as observed for Pb/TiO<sub>2</sub> (Fig. 4b). Since the Brønsted acid sites were reported to be effective for DHA dehydration into PA but

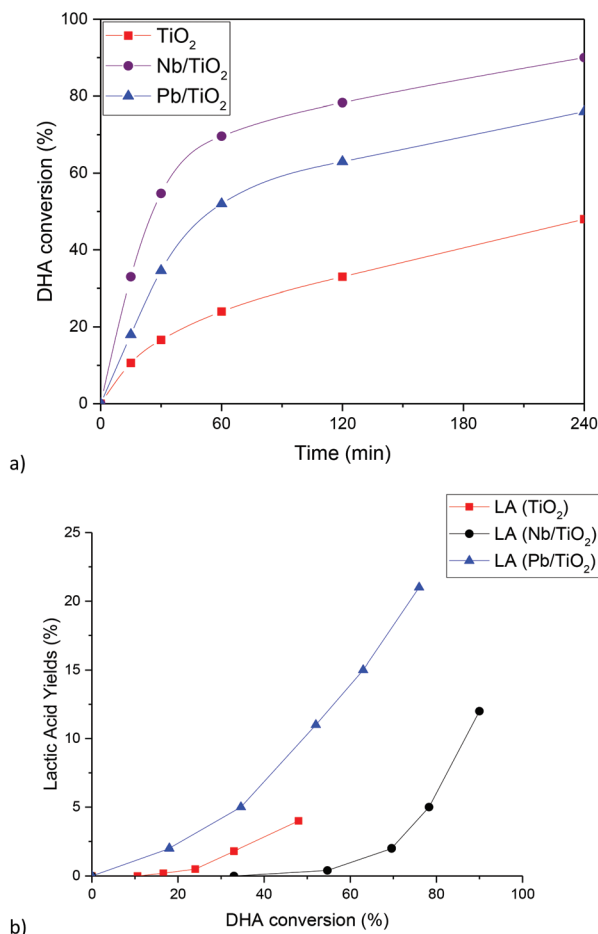


Fig. 4 (a) DHA conversion profiles as a function of time, and (b) LA yield profiles as a function of DHA conversion in the presence of undoped and doped TiO<sub>2</sub>.

Table 1 Initial rate of DHA conversion catalyzed by TiO<sub>2</sub>, Nb–TiO<sub>2</sub> and Pb–TiO<sub>2</sub>

Catalysts	TiO <sub>2</sub>	Nb–TiO <sub>2</sub>	Pb–TiO <sub>2</sub>
r <sup>o</sup> DHA consumption (mmol DHA h <sup>-1</sup> gcat <sup>-1</sup> )	5.2	14.4	8.2
S BET (m <sup>2</sup> g <sup>-1</sup> )	40	253	355

ineffective for pyruvaldehyde rehydration into LA, one can conclude that the enhanced activity of Nb/TiO<sub>2</sub> is due to an increase in its Brønsted acidity as compared to the dopant-free TiO<sub>2</sub>. The enhanced Lewis acidity of Pb/TiO<sub>2</sub> could be related to the ultra-dispersion of lead within the TiO<sub>2</sub> matrix, which would provide more efficient and accessible Lewis acid sites. Conversely, the lower dispersion of niobium within the TiO<sub>2</sub> matrix and the presence of small Nb-based clusters, as revealed by HRSTEM, could be at the origin of the Brønsted acidity. A color change of the reaction media from yellowish-white to dark brown at the end of the reaction was observed for the two most active doped TiO<sub>2</sub> catalysts, which can be attributed to the formation of oligomers as previously suggested.<sup>3,4</sup>

## Conclusions

New homo- and heteroleptic *N*-methyldiethanolamine-modified precursors of Ti(IV), Nb(V) and Pb(II) showing interesting structural diversity and sol-gel characteristics are reported. Their partial and complete hydrolysis leads to the isolation of well-defined molecular oxo-clusters or metal oxide nanoparticles, respectively, the latter forming a promising approach to obtain highly dispersed catalysts containing Nb and Pb, mainly as isolated cations within the TiO<sub>2</sub> matrix, but also as small oxo clusters of less than 2 nm on the TiO<sub>2</sub> NPs. These Nb/TiO<sub>2</sub> and Pb/TiO<sub>2</sub> catalysts with high surface areas (253–355 m<sup>2</sup> g<sup>-1</sup>) and tunable acidic properties show improved reactivity for aqueous phase dihydroxyacetone conversion.

## Author contributions

S. M. and N. E. conceived the work and supervised the materials and catalysis parts, respectively. S. M. also synthesized and characterized the precursors and wrote the manuscript. A. B. S. N. and M. G. A. C. synthesized the catalysts by the sol-gel method, characterized them and measured their catalytic activity. A. C. O. supervised the catalysis part. E. J. solved the single crystal X-ray structures of the precursors. All authors discussed the results and commented on the final manuscript.

## Conflicts of interest

There are no conflicts to declare.

## Acknowledgements

Financial support from the Capes/Brazil to A. B. S. N. (Grant No. 88881.190581/2018-01) and M. G. A. C. (Grant No. 99999.006712/2015-00) is gratefully acknowledged. The authors thank M. Aouine (HR-TEM) and Y. Aizac (XRD) of IRCELYON.

## Notes and references

- 1 A. Mansouri, R. Rihani, A. N. Laoufi and M. Özkan, *Fuel*, 2016, **185**, 612–621.
- 2 M. Hajjari, M. Tabatabaei, M. Aghbashlo and H. Ghanavati, *Renewable Sustainable Energy Rev.*, 2017, **72**, 445–464.
- 3 E. Jolimaitre, D. Delcroix, N. Essayem, C. Pinel and M. Besson, *Catal. Sci. Technol.*, 2018, **8**, 1349–1356.
- 4 S. Lux and M. Siebenhofer, *Chem. Biochem. Eng. Q.*, 2015, **4**, 575–585.
- 5 G. M. Lari, G. Pastore, M. Haus, Y. Ding, S. Papadokonstantakis, C. Mondelli and J. Pérez-Ramírez, *Energy Environ. Sci.*, 2018, **11**, 1012–1029.

- 6 S. C. D'Angelo, A. Dall'Ara, C. Mondelli, J. Pérez-Ramírez and S. Papadokonstantakis, *ACS Sustainable Chem. Eng.*, 2018, **6**, 16563–16572.
- 7 E. Pighin, V. K. Díez and J. I. Di Cosimo, *Catal. Today*, 2017, **289**, 29–37.
- 8 E. Pighin, J. I. Di Cosimo and V. K. Díez, *Mol. Catal.*, 2018, **458**, 189–197.
- 9 K.-N. T. Tseng, S. Lin, J. W. Kampf and N. K. Szymczak, *Chem. Commun.*, 2016, **52**, 2901–2904.
- 10 K. Nakajima, R. Noma, M. Kitano and M. Hara, *J. Phys. Chem. C*, 2013, **117**, 16028–16033.
- 11 (a) S. Mishra and S. Daniele, *Chem. Rev.*, 2015, **115**, 8379–8448; (b) S. Mishra, S. Daniele and L. G. Hubert-Pfalzgraf, *Chem. Soc. Rev.*, 2007, **36**, 1770–1787.
- 12 (a) S. Esposito, *Materials*, 2019, **12**, 668; (b) A. E. Danks, S. R. Hall and Z. Schnepf, *Mater. Horiz.*, 2016, **3**, 91–112.
- 13 (a) D. C. Bradley, R. C. Mehrotra, I. P. Rothwell and A. Singh, *Alkoxo and Aryloxo derivatives of Metals*, Academic Press, New York, 2001; (b) N. Y. Turova, E. P. Turevskaya, V. G. Kessler and M. I. Yanovskaya, *The Chemistry of Metal Alkoxide*, Kluwer Academic Publishers, Boston, 2002.
- 14 (a) J. Aguado, J. M. Escola, M. C. Castro and B. Paredes, *Microporous Mesoporous Mater.*, 2005, **82**, 181–192; (b) R. Akkari, A. Ghorbel, N. Essayem and F. Figueras, *J. Sol-Gel Sci. Technol.*, 2005, **33**, 121–125.
- 15 S. Mishra and S. Daniele, *Chem. – Eur. J.*, 2020, **26**, 9292–9303.
- 16 A. Verchère, S. Mishra, E. Jeanneau, H. Guillon, J.-M. Decams and S. Daniele, *Inorg. Chem.*, 2020, **59**, 7167–7180.
- 17 S. Mishra, E. Jeanneau, M. Rolland and S. Daniele, *RSC Adv.*, 2016, **6**, 1738–1743.
- 18 S. Mishra, V. Mendez, E. Jeanneau, V. Caps and S. Daniele, *Eur. J. Inorg. Chem.*, 2013, 500–510.
- 19 S. Mishra, E. Jeanneau, S. Daniele and V. Mendez, *Dalton Trans.*, 2010, **39**, 7440–7443.
- 20 S. Mishra, S. Daniele, S. Petit, E. Jeanneau and M. Rolland, *Dalton Trans.*, 2009, 2569–2577.
- 21 (a) K. E. Sanwald, T. F. Berto, W. Eisenreich, A. Jentys, O. Y. Gutierrez and J. A. Lercher, *ACS Catal.*, 2017, **7**, 3236–3244; (b) M. Hara, *Bull. Chem. Soc. Jpn.*, 2014, **87**, 931–941; (c) R. D. Clercq, M. Dusselier, C. Poleunis, D. P. Debecker, L. Giebeler, S. Oswald, E. Makshina and B. F. Sels, *ACS Catal.*, 2018, **8**, 8130–8139.
- 22 (a) K. Nakajima, J. Hirata, M. Kim, N. K. Gupta, T. Murayama, A. Yoshida, N. Hiyoshi, A. Fukuoka and W. Ueda, *ACS Catal.*, 2018, **8**, 283–290; (b) J. Wang, G. Yao and F. Lin, *Mol. Catal.*, 2017, **435**, 82–90.
- 23 T. Kemmitt, N. I. Al-Salim, G. J. Gainsford and W. Henderson, *Aust. J. Chem.*, 1999, **52**, 915.
- 24 T. Kemmit, N. I. Al-Salim and G. J. Gainsford, *Aust. J. Chem.*, 2002, **55**, 513–517.
- 25 T. Kemmitt, N. I. Al-Salim and G. J. Gainsford, *Eur. J. Inorg. Chem.*, 1999, 1847–1849.
- 26 S. Mishra, E. Jeanneau, S. Mangematin, H. Chermette, M. Poor Kalhor, G. Bonnefont, G. Fantozzi, S. Le Floch, S. Pailhès and S. Daniele, *Dalton Trans.*, 2015, **44**, 6848–6862.
- 27 (a) M. Hayatifar, F. Marchetti, G. Pampaloni and S. Zacchini, *Inorg. Chem.*, 2013, **52**, 4017–4025; (b) L. Appel, R. Fiz, W. Tyrra and S. Mathur, *Dalton Trans.*, 2012, **41**, 1981–1990.
- 28 T. Kemmitt, L. G. Hubert-Pfalzgraf, G. J. Gainsford and P. Richard, *Inorg. Chem. Commun.*, 2005, **8**, 1149–1153.
- 29 G. Mohammadnezhad, O. Akintola, W. Plass, F. Steiniger and M. Westermann, *Dalton Trans.*, 2016, **45**, 6329–6333.
- 30 A. Verchère, S. Pailhès, S. Le Floch, S. Cottrino, R. Debord, G. Fantozzi, S. Misra, C. Candolfi, B. Lenoir, S. Daniele and S. Mishra, *Phys. Chem. Chem. Phys.*, 2020, **22**, 13008–13016.
- 31 (a) A. Takagaki, H. Goto, R. Kikuchi and S. T. Oyama, *Appl. Catal., A*, 2019, **570**, 200–208; (b) K. Nakajima, J. Hirata, M. Kim, N. K. Gupta, T. Murayama, A. Yoshida, N. Hiyoshi, A. Fukuoka and W. Ueda, *ACS Catal.*, 2018, **8**, 283–290; (c) E. Jolimaitre, D. Delcroix, N. Essayem, C. Pinel and M. Besson, *Catal. Sci. Technol.*, 2018, **8**, 1349–1356.